Bioactive Materials 42 (2024) 613–627

Contents lists available at ScienceDirect

Bioactive Materials

journal homepage: www.keaipublishing.com/en/journals/bioactive-materials

Bimetallic clusterzymes-loaded dendritic mesoporous silica particle regulate arthritis microenvironment *via* ROS scavenging and YAP1 stabilization

Yang Jin [a,1], Chuan Hu [a,1], Jiechao Xia [a,1], Dingqi Xie [a], Lin Ye [a], Xinyi Ye [b], Li Jiang [c], Honghai Song [a], Yutao Zhu [a], Sicheng Jiang [a], Weiqing Li [b], Weiming Qi [f,***], Yannan Yang [d,e,**], Zhijun Hu [a,*]

[a] Department of Orthopaedic Surgery, Key Laboratory of Musculoskeletal System Degeneration and Regeneration Translational Research of Zhejiang Province, Sir Run Run Shaw Hospital, Medical College of Zhejiang University, Hangzhou, 310016, China
[b] Zhejiang University School of Medicine, Zhejiang University, Hangzhou, China
[c] Department of Biochemistry and Molecular Biology, School of Basic Medical Sciences, Hangzhou Normal University, Hangzhou, China
[d] Institute of Optoelectronics, Fudan University, Shanghai, 200433, China
[e] South Australian ImmunoGENomics Cancer Institute, Faculty of Health and Medical Sciences, The University of Adelaide, Adelaide, South Australia, 5005, Australia
[f] Zhejiang Center for Medical Device Evaluation, Zhejiang Medical Products Administration Hangzhou 310009, Zhejiang, China

ARTICLE INFO

Keywords:
Clusterzyme
Sustained delivery
Reactive oxygen species
Hippo pathway
Rabbit anterior cruciate ligament transection model

ABSTRACT

Clusterzymes are synthetic enzymes exhibiting substantial catalytic activity and selectivity, which are uniquely driven by single-atom constructs. A dramatic increase in antioxidant capacity, 158 times more than natural trolox, is noted when single-atom copper is incorporated into gold-based clusterzymes to form $Au_{24}Cu_1$. Considering the inflammatory and mildly acidic microenvironment characteristic of osteoarthritis (OA), pH-dependent dendritic mesoporous silica nanoparticles (DMSNs) coupled with PEG have been employed as a delivery system for the spatial-temporal release of clusterzymes within active articular regions, thereby enhancing the duration of effectiveness. Nonetheless, achieving high therapeutic efficacy remains a significant challenge. Herein, we describe the construction of a Clusterzymes-DMSNs-PEG complex (CDP) which remarkably diminishes reactive oxygen species (ROS) and stabilizes the chondroprotective protein YAP by inhibiting the Hippo pathway. In the rabbit ACLT (anterior cruciate ligament transection) model, the CDP complex demonstrated inhibition of matrix metalloproteinase activity, preservation of type II collagen and aggregation protein secretion, thus prolonging the clusterzymes' protective influence on joint cartilage structure. Our research underscores the efficacy of the CDP complex in ROS-scavenging, enabled by the release of clusterzymes in response to an inflammatory and slightly acidic environment, leading to the obstruction of the Hippo pathway and downstream NF-κB signaling pathway. This study illuminates the design, composition, and use of DMSNs and clusterzymes in biomedicine, thus charting a promising course for the development of novel therapeutic strategies in alleviating OA.

Osteoarthritis is a prevalent joint disorder, impacting millions globally [1]. It's a degenerative disease characterized by the gradual deterioration of the protective cartilage that cushions the joints. Subsequently, the bones within the joint directly rub against each other, leading to issues predominantly in the hand, hip, and knee joints. This results in discomfort, swelling, and stiffness. The occurrence of

Peer review under responsibility of KeAi Communications Co., Ltd.
* Corresponding author.
** Corresponding author. South Australian ImmunoGENomics Cancer Institute, Faculty of Health and Medical Sciences, The University of Adelaide, Adelaide, South Australia, 5005, Australia.
*** Corresponding author. Zhejiang Center for Medical Device Evaluation, Zhejiang Medical Products Administration Hangzhou 310009, Zhejiang, China.
E-mail addresses: qwm3140@126.com (W. Qi), yannan.yang@adelaide.edu.au (Y. Yang), hzjspine@zju.edu.cn (Z. Hu).
[1] These authors contributed equally to this work.

https://doi.org/10.1016/j.bioactmat.2024.09.004
Received 1 February 2024; Received in revised form 28 August 2024; Accepted 2 September 2024

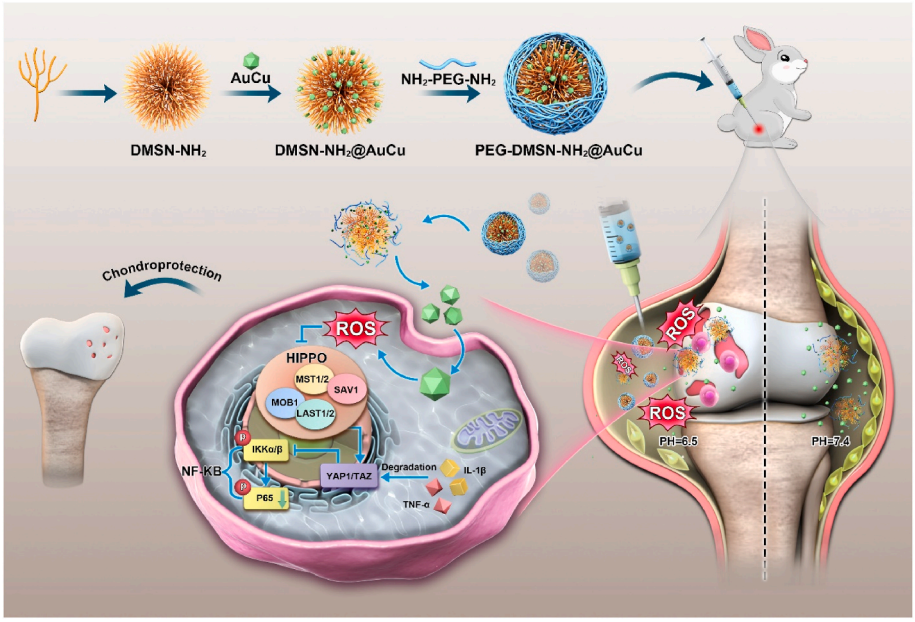

Scheme 1. Schematic illustration for the preparation of CDP and the therapeutic mechanism. The slightly acidic slow-release ability of CDP to maintain osteoarthritis microenvironment *via* ROS clearing and YAP1 protection.

symptomatic hand, hip, and knee OA experiences a steep trajectory around the age of 50, plateauing post the 70-year mark [2,3]. The progressive degradation of articular cartilage, thickening of subchondral bone, and the formation of osteophytes define OA, cumulatively leading to impaired joint mobility and reduced function.

The precipitating factors accountable for cartilage loss are multifaceted, encompassing overproduction of matrix-degrading enzymes, hastened chondrocyte hypertrophy, and localized calcification of joint cartilage. These conditions are frequently associated with an upregulation of Col10a1 and alkaline phosphatase [4,5], culminating in apoptosis and subsequent cartilage tissue destruction. In contrast, the role of Reactive Oxygen Species (ROS) in osteoarthritis has been extensively explored. Heightened ROS levels can dismantle the extracellular matrix (ECM) and chondrocytes, cells vested with the responsibility for ECM synthesis and upkeep, resulting in a decline in chondrocyte viability and ECM decomposition. ROS also has the potential to activate matrix metalloproteinases (MMPs), enzymes that degrade ECM constituents [6–8], further exacerbating cartilage breakdown. Moreover, ROS can induce chondrocyte apoptosis, leading to ECM synthesis reduction and ultimately cartilage loss. Consequently, comprehending and targeting the mechanism through which ROS stimulates cartilage damage is pivotal to devising effective osteoarthritis treatments.

In recent times, nanozymes have emerged as a promising substitute to natural enzymes, which are hampered by limited environmental tolerance, high cost, and labor-intensive preparation processes. These synthetic enzymes offer several benefits over their natural counterparts, including cost-effectiveness, robust catalytic stability, and easy modifications [9–11]. However, their utility has been restrained by limitations such as lack of catalytic selectivity and uncontrollable modulation [12]. Atom manipulation *via* atomic engineering represents a viable solution to this, as it can enhance catalytic activity and selectivity at atomic scales [13]. The abundance of transition metal electronic states and a plethora of electronic energy levels render gold-based materials a robust foundation for designing atomic-scale enzymes. These materials have demonstrated various enzyme-like activities, such as those exhibited by peroxidase (POD), catalase (CAT), and superoxide dismutase (SOD) [14]. By leveraging delicate single-atom substitutions *via* copper modulation, we can achieve enzymatic selectivity, ultra-high antioxidant activity with rapid kinetics, hence yielding exceptional properties suitable for treating inflammatory diseases. However, drugs administered into the articular cavity are rapidly flushed out by the synovial lymph nodes and vascular system. Hence, enhancing the retention rate of drug formulations within the articular cavity can potentially improve their efficacy [15]. The strategies for achieving sustained drug delivery remain an area of active research.

The protective effects of nanozymes can be harnessed through the utilization of drug-loading systems. Dendritic Mesoporous Silica Nanoparticles (DMSNs) represent a type of nanomaterial that has drawn extensive interest of late due to their distinctive properties and potential applications [16]. DMSNs are constitutively a silica core enveloped by a dendritic structure, yielding a broad surface area and a complex pore network [17,18]. This unique structure renders DMSNs suitable for diverse applications, including drug delivery, catalysis, and sensing. The capacious surface area and the porous configuration of DMSNs allow for high drug loading and sustained release, thereby enhancing drug efficacy and mitigating side effects [19]. Additionally, the dendritic structure of DMSNs can be functionalized with targeting ligands, facilitating targeted drug delivery to specific cells or tissues. Most importantly, the incorporation of new chemical bonds during synthesis can impart responsive properties, such as ROS, GSH, pH, to DMSNs [20]. Consequently, pH-dependent DMSNs were utilized to encapsulate clusterzymes.

In this study, we assembled a pH-dependent system by loading clusterzymes in DMSNs (PEG-DMSNs-NH_2@AuCu, abbreviated as CDP). Utilizing the microenvironmental attributes of osteoarthritis (OA), we harnessed this reaction release structure to enhance the retention efficiency of clusterzymes in joints. When inflammation arises, the slightly acidic microenvironment triggers the pH-dependent release of clusterzymes. Through this spatio-temporal delivery, reactive oxygen species (ROS) in osteoarthritis are effectively cleared, subsequently improving the inflammatory microenvironment and safeguarding joint cartilage. CDP showcases exceptional ROS-scavenging activity *in vitro* and additionally reduces the manifestation of cartilage-destruction-related proteins such as ADAMTS and MMP. Moreover, CDP has demonstrated an ability to attenuate the progression of OA in *vivo* without notable toxicity, thereby presenting a promising strategy for the treatment of OA. We anticipate that this study will pave the way for new

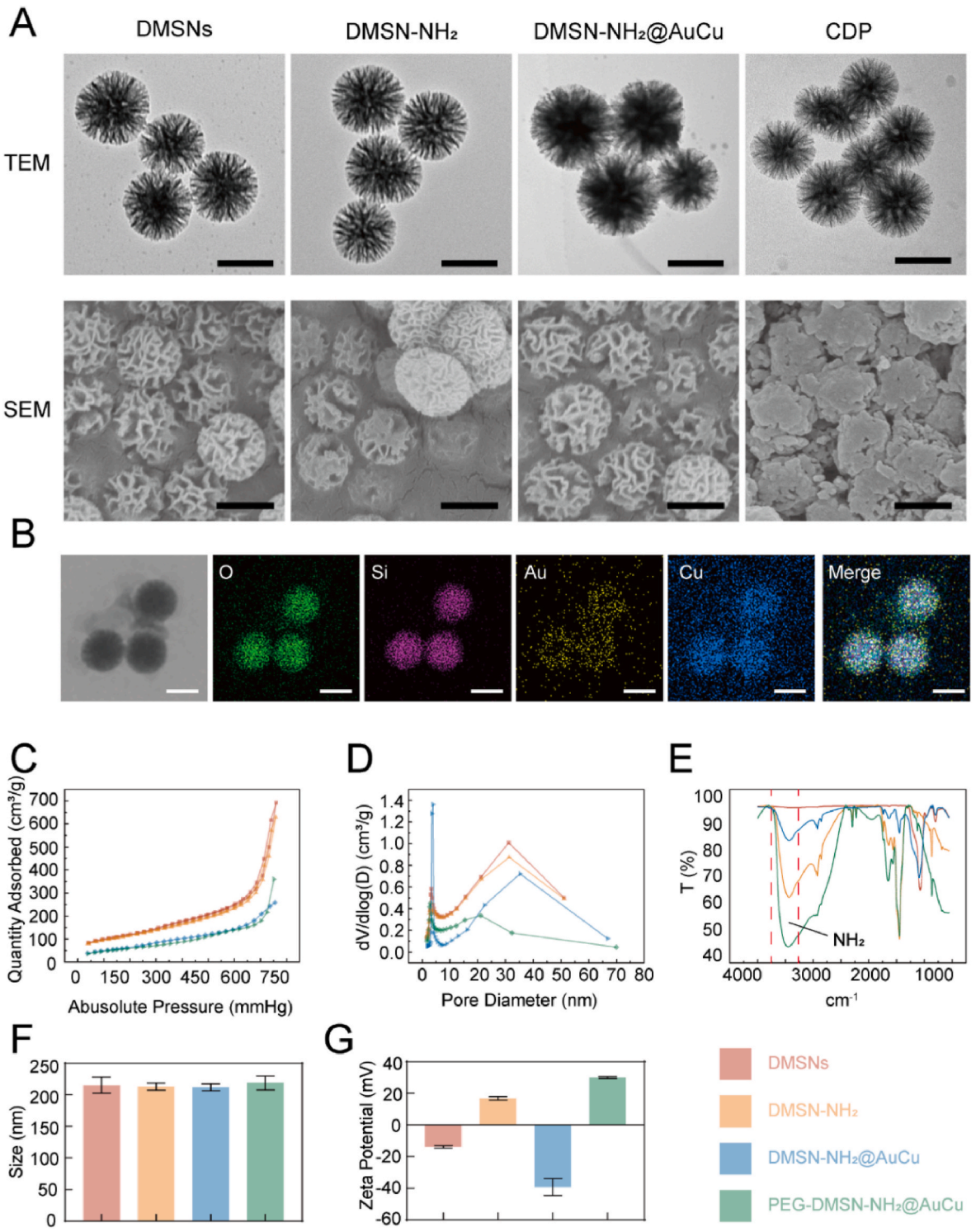

Fig. 1. Preparation and Characterization of CDP. A) TEM and SEM images of DMSNs, DMSNs-NH_2, DMSNs-NH_2@AuCu, CDP; scale bar = 200 nm. B) Corresponding area-elemental mappings of the CDP; scale bar = 200 nm. C-D) N_2 adsorption−desorption isotherm and pore size distribution of CDP and its' elements. E) FT-IR, F) Particle size differences and G) zeta potential of CDP and its' elements show the positive potential makes CDP loading successfully.

opportunities centered on the application of novel clusterzymes in preventing and treating ROS-associated diseases.

1. Results and discussion

The CDP system devised in the current research embodies a promising strategy for treating osteoarthritis (OA). Nanodrug delivery systems have shown great potential to prolong intra-articular residence, penetrate the ECM, and achieve diseased chondrocyte-specific delivery [21]. As depicted in Scheme 1, this system comprises dendritic mesoporous silica nanoparticles (DMSNs) which are modified with 3-aminopropyltriethoxysilane (APTES) and then enveloped with polyethylene glycol (PEG). DMSNs have earned considerable acknowledgment as drug delivery systems due to their superior loading capacity and sustained release attributes. The surface of DMSNs, when modified with APTES, acquires a positive charge, thus favoring the incorporation of

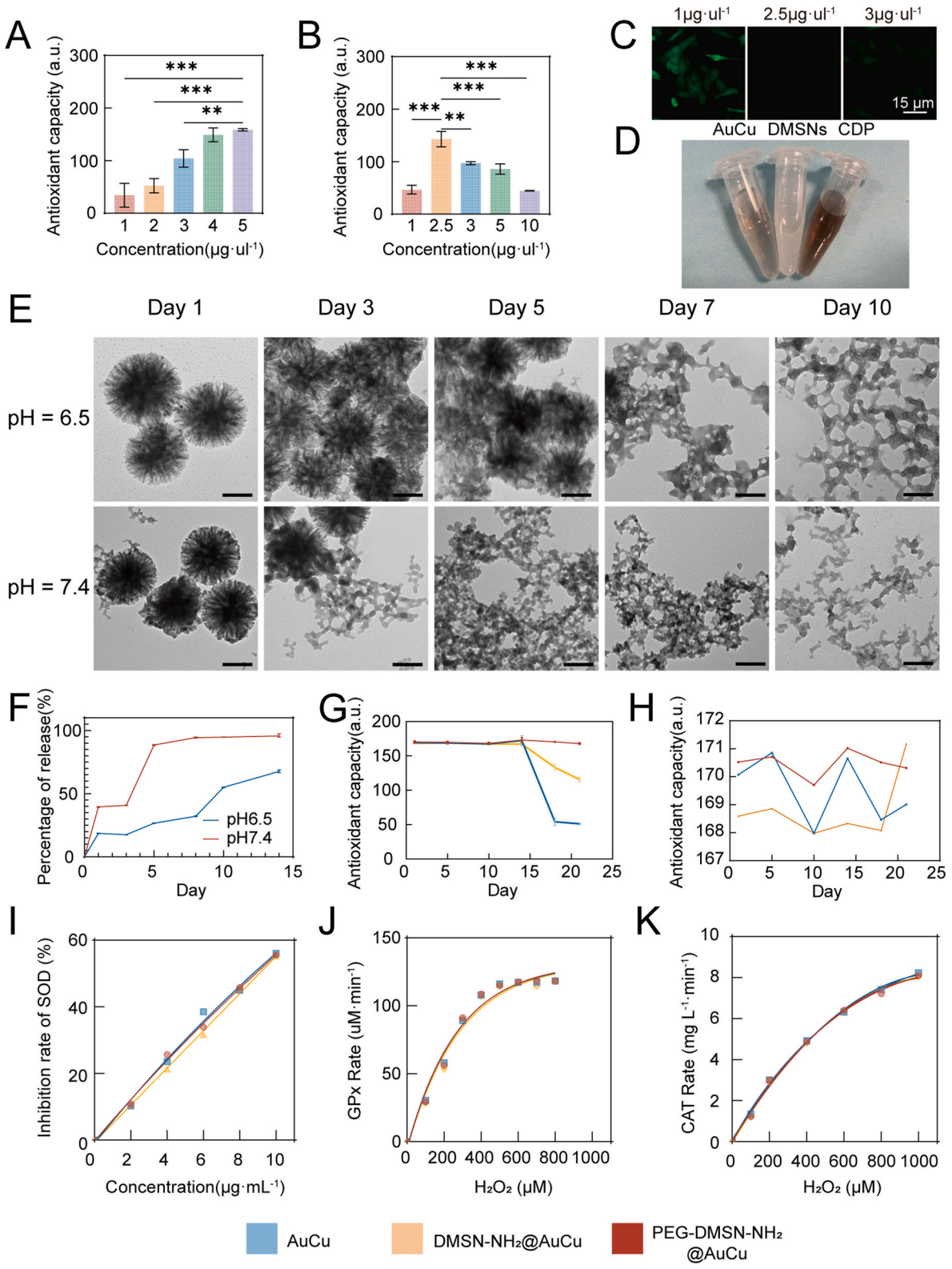

Fig. 2. A) antioxidant capacities of $Au_{24}Cu_1$ Clusterzymes and B) Concentration-dependent (1–10 ng/ul) of DMSN guaranteed the capacities. C) Comparison of antioxidant activity of 3 ratios of CDP in cell species. D) Outlook of Clusterzymes, DMSNs and CDP. E) TEM images of DMSNs-NH_2 after biodegradation in neutral (pH = 7.4) and acidic (pH = 6.5) SBF for varied durations; scale bar = 100 nm. F) Release of $Au_{24}Cu_1$ Clusterzymes within CDP after biodegradation in neutral (pH = 7.4) and acidic (pH = 6.5) SBF for varied durations. G) Antioxidant capacity stability of CDP and its' elements for varied duration H) in neutral (pH = 7.4) and acidic (pH = 6.5) SBF. The I) SOD, J) GPx and K) CAT-like activity of clusterzymes, DMSNs-NH_2@AuCu and CDP. (**: $p < 0.01$, ***: $p < 0.001$).

negatively charged drugs, such as the ROS-consuming clusterzymes utilized in our study. The NH_2-PEG-NH_2 coated DMSNs display improved biocompatibility and successfully avoid opsonization by serum proteins [22], thereby elongating their half-life *in vivo*.

Designed with pH-dependent, the CDP system allows DMSNs to disintegrate at a slower pace in the acidic microenvironment of OA, thereby accomplishing the spatiotemporal delivery of clusterzymes. This responsive drug delivery approach holds the potential to mitigate ROS stress and inflammation in the affected joint while also offering protection to the articular cartilage. For comparison purposes, a control system was prepared, comprising DMSNs coated solely with NH_2-PEG-NH_2 (NH_2-PEG-DMSNs) and clusterzymes diffused in PBS. The CDP

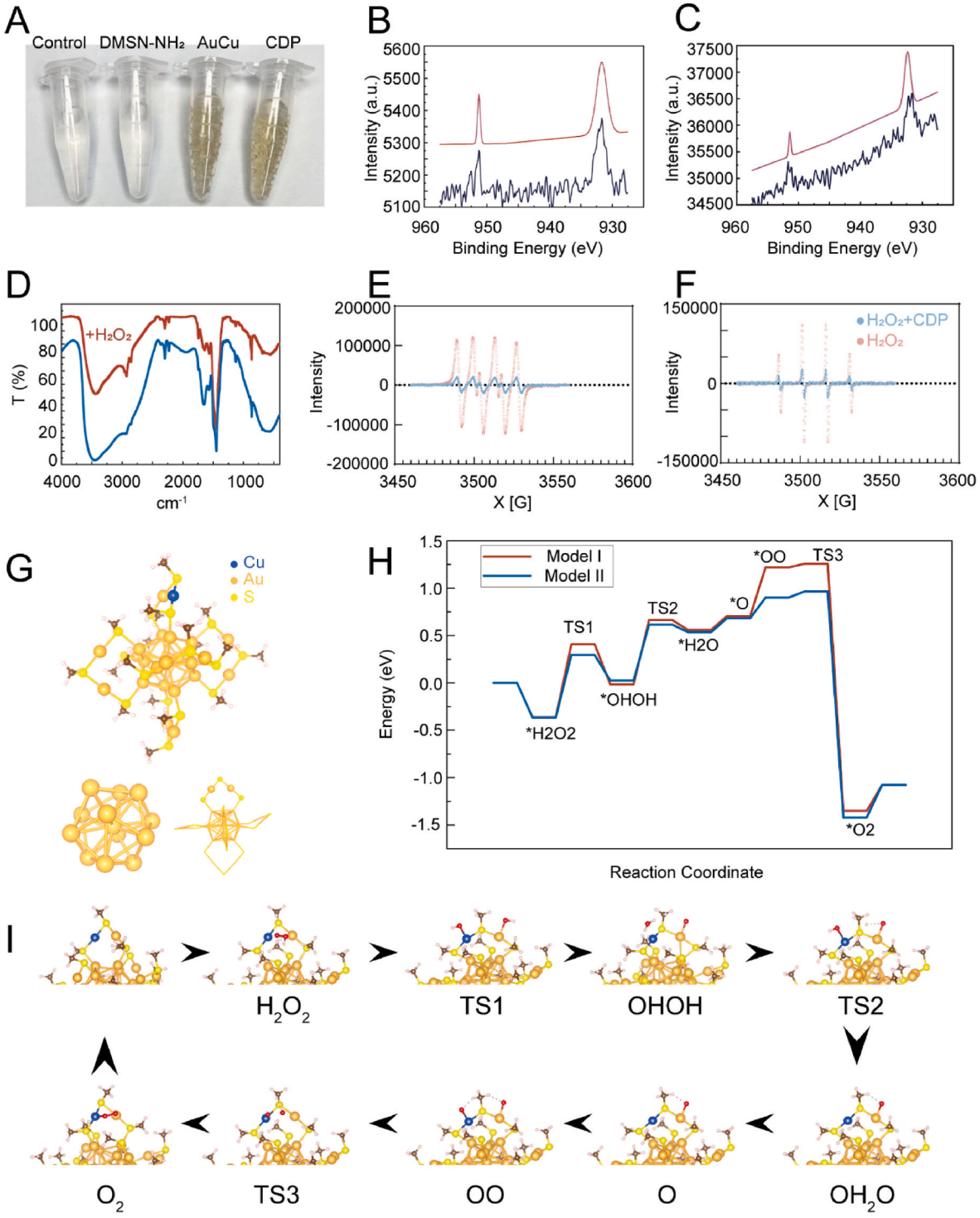

Fig. 3. Calculation of Clusterzymes and measurement of CDP. A) Outlook of antioxidant capacity after CDP and its' elements were put into 3 % H_2O_2. XPS of $Au_{24}Cu_1$ Clusterzymes B) at the beginning and after C) 3 weeks. D) FT-IR of clusterzymes before and after it was put into 3 % H_2O_2. E) •OH and F) $O_2^{\bullet-}$ studied by the ESR spectroscopy. BMPO is used as the ROS-capturing agent and the sources of •OH and $O_2^{\bullet-}$ are H_2O_2 and KO_2, respectively. G) the structure of $Au_{24}Cu_1$ clusterzymes, with core (left bottom) and side chain (right bottom). H) energies profiles of catalytic process of SOD processes compared with Au_{25} and I) charge analysis of $Au_{24}Cu_1$.

system outperformed its counterpart, demonstrating superior efficacy in curtailing ROS stress and inflammation both *in vitro* and *in vivo*. These results suggest its potent potential to serve as a promising therapeutic regimen for OA.

2. Synthesis of CDP

We prepared DMSNs deploying cetyltrimethylammonium bromide (CTAB) and sodium salicylate (NaSal) as structure-directing agents, tetraethyl orthosilicate (TEOS) as a silica source, and triethylamine (TEA) as a catalyst [17]. Further, we functionalized them with amino groups to confer a positive surface charge that would facilitate the loading of clusterzymes. Lastly, we sealed the mesoporous void with NH_2-PEG-NH_2 [23,24], culminating in the creation of the DMSNs. We examined these resulting DMSNs and monitored their changes post-clusterzymes loading using scanning electron microscopy (SEM) and transmission electron microscopy (TEM). The analysis confirmed their uniform particle size and mesoporous structure (Fig. 1A). The particle size of the DMSNs spanned from 190 to 230 (±20 nm) nm, while the mesopores displayed widths between 2 and 50 (8 ± 11) nm, a range that support the loading of clusterzymes (Fig. 1B and Fig. S1, Supporting Information). We validated the mesoporous structure of DMSNs through type IV nitrogen adsorption-desorption isotherm analysis, which exhibited a broad peak centered at 31.17 nm in the corresponding Barrett, Joyner, and Halenda (BJH) pore size distribution curve. Following the encapsulation of clusterzymes, a decline was observed in the type IV nitrogen adsorption-desorption isotherms and an indistinct peak was displayed in the group of CDP; a group that is twined on the surface of DMSNs by NH_2-PEG-NH_2 (Fig. 1C and D). The FT-IR highlighted differences in the amino absorption peak, found in the 3200-3500 cm^{-1} range, between the amino-functionalized DMSNs and those with NH_2-PEG-NH_2 on the surface (Fig. 1E). Concurrently, there were no marked differences in the particle sizes among the 4 groups (Fig. 1F), indicating that the clusterzymes were not adhered to the surface but stowed within the pores.

To maximize the loading capacity of clusterzymes [25], we synthesized clusterzymes inside the mesoporous structure of DMSNs. Given that the dimensions of clusterzymes are under 5 nm, their loading would remain uninfluenced. However, the negative potentials of both DMSNs and clusterzymes present a challenge in loading an adequate quantity of clusterzymes into the DMSNs. To address this, the DMSNs' surface was modified with amino groups, thereby forming DMSNs-NH_2. This molecule possesses a positive potential, allowing it to attract the negatively charged clusterzymes [26], thereby enhancing the loading capacity. Yet, for facilitating cellular uptake, it was necessary to retain this positive potential. Hence, we modified PEG with amidogen, leading to the creation of a positively charged surface and pore-sealing material. This modification permitted the newly christened PEG-bound DMSNs-NH_2-Clusterzyme (CDP) to keep its positive charge, easing the internalization of the drug-loaded system by cells. Simultaneously, it acted as a sealing material, curtailing drug-leakage during the delivery cycle. Existing evidence suggests that the use of PEG to modify DMSNs' surfaces boosts the system's biocompatibility and optimizes cellular uptake (Fig. 1G).

During the loading process, we paid particular attention to whether the inherent properties of clusterzymes would be altered and if they could respond to stimuli for release. Evaluating the antioxidant properties of clusterzymes and CDP was deemed necessary. In addition, we sought to determine the maximum load of DMSNs that could be achieved. An earlier study spotlights the ROS scavenging ability of clusterzymes [13], which is further enhanced with the supplementary inclusion of a Cu atom, as corroborated by material characterization findings. To this end, our research discovered that the antioxidant activity of $Au_{24}Cu_1$ superseded that of Trolox by a factor of 158, as per quantitative results (Fig. 2A) [27,28]. The loading of clusterzymes into DMSNs-NH_2, along with the concentration of DMSNs-NH_2 during synthesis, could influence the antioxidant capacities of CDP. An examination of the DMSNs-NH_2 concentration gradient revealed that the optimal concentration for CDP was 2.5 ng/μl (Fig. 2B). The antioxidant performance of different ratios of CDP in hydrogen peroxide stimulated C28/I2 cartilage cell lines also demonstrated the reliability of the optimal ratio (Fig. 2C). Moreover, the color of CDP darkened when compared to the paler clusterzymes and the white DMSNs-NH_2 (Fig. 2D).

2.1. Antioxidant and release properties of CDP

The pH-dependent nature of DMSNs plays a significant role in the release of clusterzymes. Our laboratory experiments indicate the biodegradation behavior of DMSNs under both subacid and neutral conditions. Fig. 2E shows that DMSNs display pH-dependent degradation behavior. Notably, they degrade more slowly in mildly acidic conditions (pH 6.5) compared to neutral settings (pH 7.4) [29], which makes them suitable for CDP retention in a slightly acidic joint fluid environment. This characteristic comes from the hydrolysis of the siloxane bonds in the DMSNs structure, catalyzed by OH^-. DMSNs' ability to degrade in acidic environments heralds their potential as a targeted drug delivery system for diseased tissues featuring acidic microenvironments, as seen in conditions like osteoarthritis. Moreover, CDP can transport drugs in a spatiotemporal manner in acidic settings to maintain their long-term therapeutic effectiveness on localized lesions.

We proceeded to examine the release pattern of clusterzymes in dual pH conditions: the typical joint environment (pH = 7.4) and a slightly acidic arthritic environment (pH = 6.5), maintaining a consistent concentration. The percentage of clusterzymes released was tracked over a fortnight using inductively coupled plasma-mass spectrometry (ICP-MS) (Fig. 2F) [30]. The DMSNs-NH_2 feature influenced the release of clusterzymes over time. A slower release was visible in the mildly acidic ambiance, potentially extending the protection window for articular cartilage. In light of the clusterzymes' expiration limit, we collected the supernatant of the CDP for an extra week to measure antioxidant capacity. Our tests revealed no significant changes in antioxidant capacity, suggesting that PEG and DMSNs-NH_2 could effectively store clusterzymes. On the flip side, clusterzymes in a mildly acidic environment demonstrated reduced antioxidant potency, whether isolated or sans PEG (Fig. 2G and H). Concurrently, all specimens exhibited a preference for enzyme-mimicking catalytic procedures, with Clusterzymes, DMSNs-NH_2@AuCu, and CDP revealing compelling selectivity in their glutathione peroxidase-like (GPx-like), catalase-like (CAT-like), and superoxide dismutase-like (SOD-like) activities, respectively (Fig. 2I, J, and K).

In conclusion, CDP leverages the high ROS scavenging efficacy of low doses of $Au_{24}Cu_1$ clusterzymes. This approach enables the extension of the ROS-scavenging duration without negatively impacting the properties.

2.2. DFT calculations and the mechanism of catalytic selectivity

The antioxidant capacity was evident under 3 % H_2O_2 conditions, with numerous bubbles appearing in both groups containing clusterzymes (Fig. 3A). Consequently, we carried out an analysis on the variations within the Cu 2p X-ray Photoelectron Spectroscopy (XPS) spectrum to ascertain the structure and attributes of the clusterzymes. The double peaks spotted in the spectrum signified that the structure and characteristics of the clusterzymes remained consistent (Fig. 3B and C). This conclusion was confirmed by comparing the FT-IR before and after exposing the clusterzymes to 3 % H_2O_2. We proceeded with a further investigation of the specific scavenging of free radicals by CDP. After just 10 min, the ESR signals of •OH and $O_2^{\bullet-}$ in the control group suggested an excess of ROS. This was considerably diminished in the CDP group, pointing to an impressive scavenging efficiency (Fig. 3E and F).

We elucidated the catalytic mechanism of clusterzymes by conducting Density Functional Theory (DFT) calculations to study the

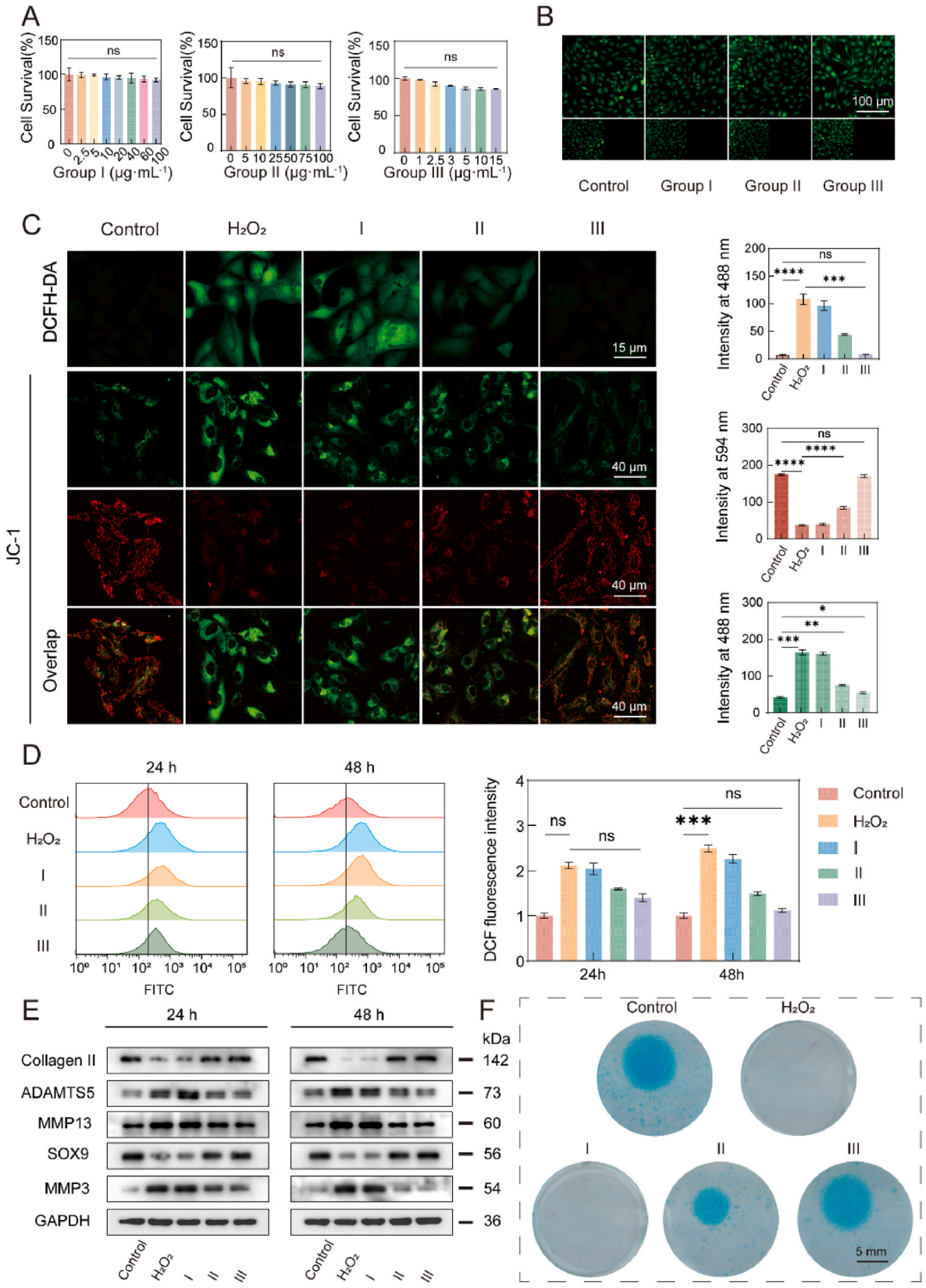

Fig. 4. *In vitro* cell assay of CDP with C28I2 chondrocyte. A) CCK8 and B) Live/dead staining of C28I2 co-culture with CDP or its element after 48 h. C) ROS scavenging activities (first row) and mitochondrial function salvage (the last three rows) in C28I2 and polymer Fluorescence density analysis. D) Flow cytometry reveal CDP rescue C28I2 under 1 mM H_2O_2 stimulate after 24 and 48 h. E) Western blotting for Collagen II, ADAMTS5, MMP13, SOX9 and MMP3 with treatment after 24 and 48 h (n = 3 per group). F) Alcian blue stain of C28I2 after 24 h (*: $p < 0.05$, **: $p < 0.01$, ***: $p < 0.001$, ****: $p < 0.0001$).

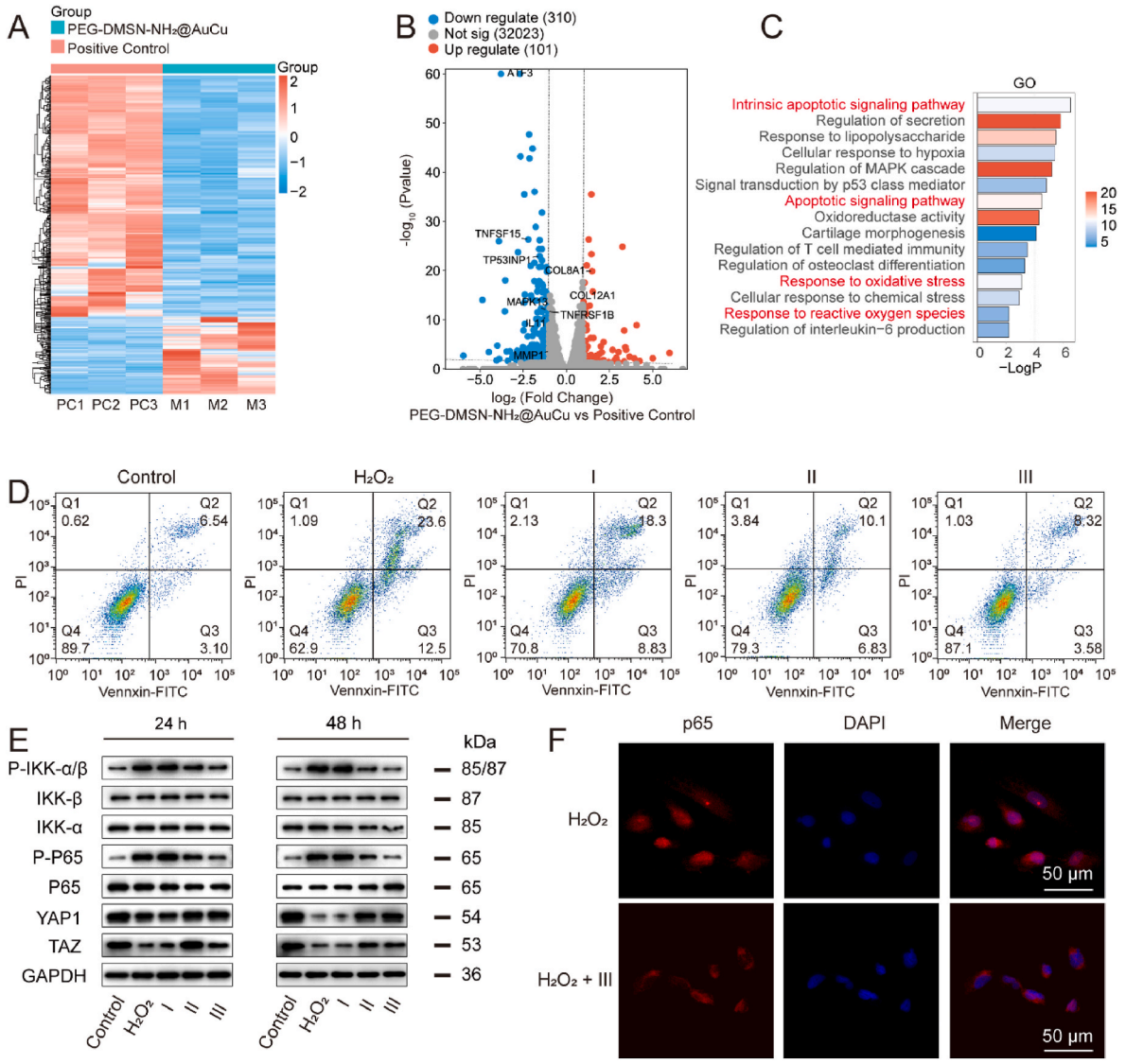

Fig. 5. RNA – Seq of 1 mM H_2O_2 stimulate C28I2 with or without CDP. A) heat map of Positive Control and CDP group. (n = 3). B) Gene which regulated after treatment. C) GO enrichment bar plots. (hippo signaling pathway) D) Apoptotic flow cytometry of C28I2 treated with 1 mM H_2O_2 and CDP or its' elements (groups I - III) compared with control groups. E) Western blotting for YAP1, TAZ, phosphor – IKK α/β and P65. F) Inhibition of P65 enucleate after treated with CDP.

catalytic selectivity and quantum features [31,32]. Earlier research has proposed various structures for clusterzymes. For our study, we adopted the model of $Au_{24}Cu_1$ clusters having a golden core safeguarded by ligands adjoined to the core *via* S atoms. The cluster was segmented into a core of Au_{13}, alongside six side chains of Au_2S_3. One Au atom on one side chain was substituted with a Cu atom (Fig. 3G).

The outstanding ROS scavenging ability of clusterzymes can be explained by the following reaction mechanism (Fig. 3H and **I**). Initially, H_2O_2 is adsorbed near the metal atom in the side chain to form · H_2O_2. Since there is no direct bonding between H_2O_2 and the metal atom, the adsorption energy remains constant even after the replacement of Au with Cu. In the second step, H_2O_2 is decomposed into two OH, which then bind to different metal atoms with different side chains, forming two ·OH. Next, the O atom of one ·OH transfers to the other, resulting in the formation of ·O and · H_2O. The ·O then combines with another ·O to form ·O_2, while losing an electron like · H_2O. Finally, the clusterzymes returns to its original state. Overall, under the catalytic action of clusterzymes, H_2O_2 is decomposed into O_2 and H_2O at a rapid rate. This catalytic mechanism has been elucidated through density functional theory (DFT), which has been utilized to investigate the catalytic selectivity and quantum properties of clusterzymes in previous studies.

During the catalytic process, the advantage of Cu replacement could be proved by charge analysis [33]. The electron loss of Au atom is about 0.05e, while that of Cu atom is 0.37e, indicating that Cu has a better ability to provide electrons. In the charge-difference diagram, the larger green area around Cu indicates that more electrons are transferred to the position between Cu-S, which is consistent with the worse charge result. After H_2O_2 is decomposed into •OH, $Au_{24}Cu_1$ loses more electrons, indicating that the charge is transferred from Au to •OH. The electron loss of Cu atom in $Au_{24}Cu_1$ is about 0.65e, more than that of Au atom (about 0.42e), and about 0.35e of Au in Au_{25} (the corresponding electron gain on the O atom has a similar trend), indicating that the effect of $Au_{24}Cu_1$on •OH is stronger than that of Au_{25}, and Cu is better than Au. When H_2O_2 is converted to •O and •H_2O, the H atom is transferred from Au to Cu, the Au-O bond is strengthened and the bond between Cu-O is weakened. The adsorption of H_2O molecules is not strong, H_2O are able to desorb quickly with no atomic charge change. After the two •O bonded to form O_2 molecule, most of the electrons obtained from the oxygen atom returned to the clusterzymes. However, in $Au_{24}Cu_1$, there was still about 0.59e charge loss on the Cu atom, most of which was distributed on the O_2 molecule (O1:0.25e, O2:0.20e), certified that Cu and O_2 molecules still had some interaction (Tables S1–9, Supporting

information).

2.3. Modulation of oxidative stress in vitro

Amid the progression of arthritis and associated inflammatory disorders, ROS get produced, leading to cell signaling pathway disturbances, and mitochondrial dysfunction in chondrocytes [34]. To gauge the biocompatibility and ROS scavenging prowess of CDP in chondrocytes, we utilized the C28I2 chondrocyte line for *in vitro* testing [35]. Initially, we checked the cell toxicity of CDP (group III), and its constituents, DMSNs-NH_2@AuCu (group II) and clusterzymes (group I), showing no significant variation between groups after 48 h of incubation, at a density of 10 ng/μl through CCK-8 and cell death staining, (Fig. 4A and B). CDP was almost wholly consumed by cells within 12 h and it co-locates with lysosome after 24 h, thereby confirming the entire process of CDP entering the cell and being eliminated. (Fig. S2B, Supporting information). We recreated a high ROS environment by incubating C28I2 cells with a medium containing 1 mM H_2O_2 for 24 h, afterwards adding CDP into the medium for another 24 h. ROS staining by DCFH-DA disclosed the notable ROS scavenging prowess of group III, while group II demonstrated a slightly weaker ROS scavenging capability. Additionally, we scrutinized the state of the cells post ROS simulation by assessing mitochondrial membrane potential, sensitized to peroxidation. The potential, in group III, was preserved at a normal level, protected by CDP as evidenced by potent red fluorescence and weak green fluorescence due to JC-1 amassing in the mitochondria matrix. The maintenance of mitochondrial membrane potential under high ROS circumstances verifies the ROS scavenging ability of CDP (Fig. 4C). On the whole, confocal imaging and statistical outcomes demonstrate that CDP serves as an efficient oxidative modulator *in vitro*. We further explore the ROS-scavenging ability of CDP with DCFH-DA employed as the ROS indicator. This agent facilitated the detection of intracellular oxidative stress in C28I2 cells that were stimulated with 1 mM H_2O_2 for 24 h. The DCFH-DA reagent could infiltrate the cell membranes and cleaved into DCFH. The DCFH was then oxidized into DCF that carries a fluorescence imaging function. The fluorescence intensity was evaluated *via* flow cytometry analysis. To examine the intensity modification after 24 or 48 h, group III, or its constituent group II, and group I were included (Fig. 4D).

Initially, there was no significant difference after 24 h, with the peaks of group III and the H_2O_2 group both shifting to the right, suggesting chondrocytes' sensitivity to ROS stimulation induced by H_2O_2. From the degree of migration in the 24-h group, a preliminary evaluation of the ROS resistance trend for the 3 groups can be made, with group III appearing to be the most effective. Yet, the differences began to emerge significantly 48 h after dosage introduction. Both CDP and clusterzymes succeeded in maintaining normal fluorescence intensity, indicating their capacity to control ROS levels. Conversely, a persistently high ROS pressure exceeded the regulatory capacity of chondrocytes in group I and positive control groups. This resulted in a noticeable enhancement in the fluorescence intensity and a shift in the peak to the right.

The expression of catabolic enzymes like matrix metalloproteinases-3 (MMP3) and ADAMTS5, as well as anabolism-related proteins such as Sox9 and Col2A1 [36,37], play a key role in regulating cartilage decay and chondrogenesis in arthritis. To explore the protective effect of CDP on chondrocytes, we employed western blotting (Fig. 4E and Fig. S3, supporting information). In order to mimic the high ROS microenvironment seen in arthritis, DMEM medium supplemented with 1 mM H_2O_2 was used for 24 h. Interestingly, in the H_2O_2 and group I, the expression of anabolism-related proteins (collagen II and SOX9) was notably reduced while the catabolism-related protein MMP3 was upregulated. It's worth to mention that the differences were not significant in the first 24 h, such as MMP3 and Sox9, but became sharper when the incubation period was extended to 48 h, signifying that CDP showcased protective effects at the protein level after 24 h, aligning with the results of flow cytometry. Additionally, group II displayed similar results to group III, however, aspects like a slow-release system and surface charge might have affected its efficacy, leading to a lesser difference from the positive control when compared to group III. Using Alcian blue staining, we could more directly observe the disparities in type II collagen production (Fig. 4F). Under the influence of 1 mM H_2O_2 stimulation, type II collagen production couldn't be maintained while both group II and group III had clusterzymes for ROS scavenging, shown by a large blue area. By comparing group II and group III, similar conclusions can be drawn as with western blotting, *i.e.*, the slow-release system and surface charge may have impacted its efficacy in cell uptake and ROS scavenging efficiency.

2.4. RNA sequencing of CDP-treated chondrocyte

To further showcase the capability of CDP to alleviate ROS-induced stress and regulate molecular pathways, we conducted RNA sequencing to profile the transcriptome of chondrocytes treated with 1 mM H_2O_2 and CDP (Fig. 5A). We marked upregulated genes such as col8a1 and col12a1, and downregulated genes including MMP1, IL11 and MAPK13 (Fig. 5B) [38]. Gene ontology (GO) analysis revealed a robust correlation of CDP with intrinsic apoptotic signaling pathway, apoptotic signaling pathway, response to oxidative stress, and response to reactive oxygen species, particularly the hippo pathway (Fig. 5C and Fig. S4, Supporting information). As a result, we initially determined the impact of CDP on apoptosis through apoptotic flow cytometry. The level of cell apoptosis in each group was analyzed by apoptosis analysis *via* flow cytometry. The rates of both late apoptotic cells (Q2) and early apoptotic cells (Q3) considerably surged (from 9.64 % to 36.10 % total) when treated with only clusterzymes, whereas treatment with CDP further dwindled the apoptosis rate (from 11.90 % to 16.93 % total) (Fig. 5D). In short, the results presented above portray the exceptional performance of CDP in terms of anti-apoptosis *in vitro*.

2.5. CDP scavenges excess ROS to inhibit hippo pathway activation for chondroprotection

In arthritis, elevated levels of ROS can damage cartilage in several ways [39]. One such mechanism involves excessive ROS eliciting oxidative stress, which in turn activates the hippo pathway and inhibits YAP/TAZ nuclear translocation [40]. Inflammatory factors and excessive Reactive Oxygen Species (ROS) associated with arthritis lead to the activation of LATS1/2 kinase in the Hippo pathway. This, in turn, directly phosphorylates YAP1/TAZ. The cytoplasmic retention and degradation of SCF/β-TRCP E3 ubiquitin ligase happen under various stimuli. For instance, trauma-triggered inflammation activates WWC protein and changes in joint cavity stress caused by osteoarthritis also influence Hippo pathway activation [41,42]. Moreover, YAP1 can possibly rejuvenate aging hMSC, delaying the progression of osteoarthritis through the activation of cooperative expression of a neuroprotective protein named FOXD1 [43]. Preservation of articular cartilage is linked with YAP activation, whereas loss of YAP in chondrocytes tends to promote cartilage destruction [44]. Connecting these findings with our sequencing results, we speculated that CDP may guard YAP by scavenging ROS which consequently protects the articular cartilage [45]. To validate this hypothesis, we measured the protein levels post-stimulation with 1 mM H_2O_2. In the H_2O_2 and group II, YAP/TAZ degradation was noticeable. Yet, degradation was successfully thwarted in the clusterzymes and CDP groups (Fig. 5E and Fig. S5, Supporting information). These findings align with earlier observations indicating that CDP effectively improves the scavenging effect on ROS and sustains stability over time when compared to clusterzymes.

Next, we investigated the impact of YAP protection on downstream signaling pathways, especially the inflammation-associated NF-κB signaling pathway, which is a complex element in OA pathogenesis [46]. It's been demonstrated that excessive ROS or inflammatory cytokines, such as TNFα and IL-1β, play roles in cartilage decay through the NF-κB

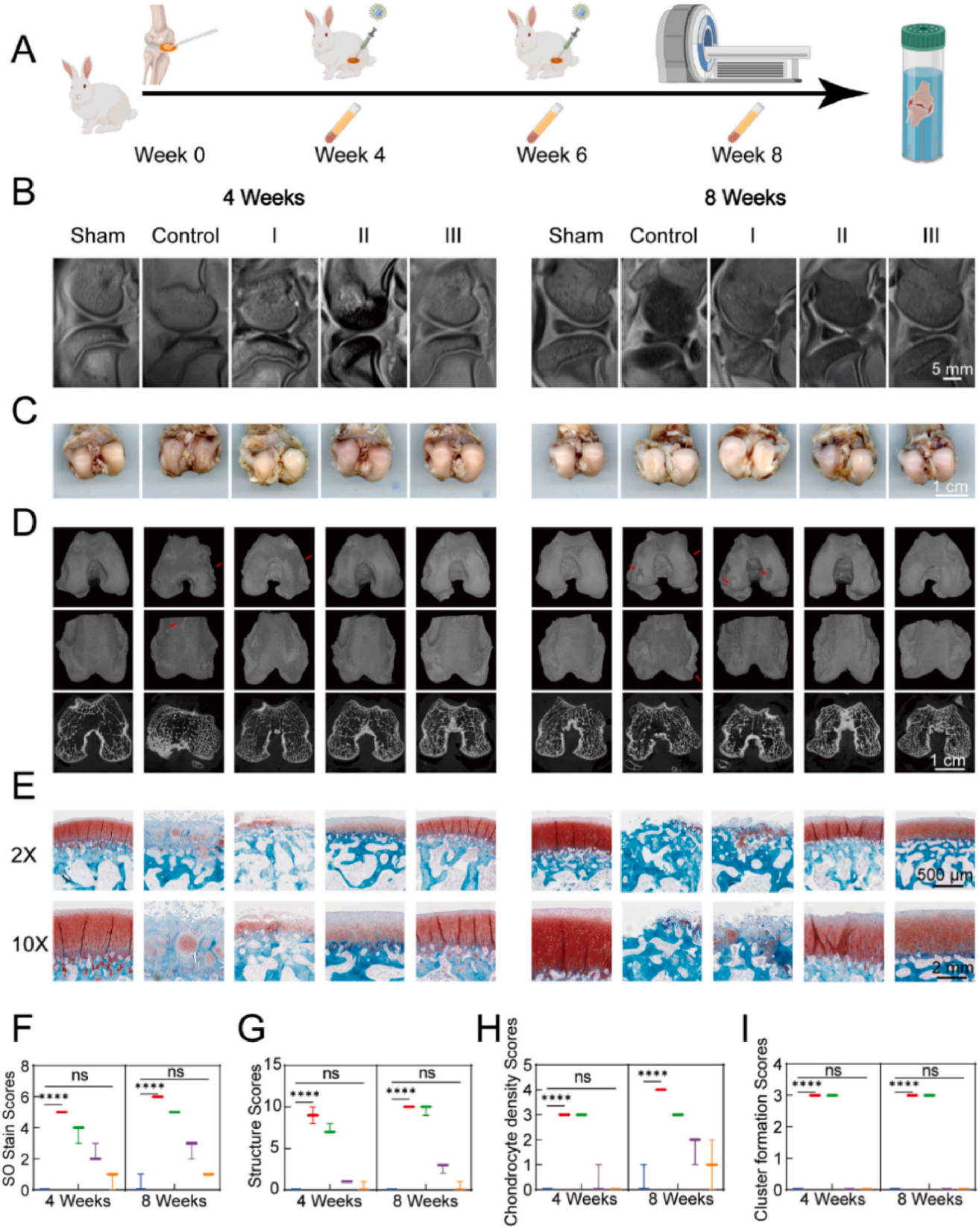

Fig. 6. *In vivo* experiment of CDP on rabbits. A) Process of groups divided by time or treatment stage, aiming to verify controlled release and protect functions of CDP. B) Magnetic resonance imaging of every group before end point. (n = 3 per group), OA group shows severe destruction of articular structure after 8 weeks, which could be rescued with CDP. C) The outlook surface of caput femoris.D) Micro-CT of caput femoris. Osteophyte is observed in control and group I, (indicated by red arrows) which is another evidence prove that CDP can delay OA progress. E) Representative images from Safranin O/Fast Green staining of medial femoral condyles, the images are assessed by OARSI score from F) SO stain, G) structure, H) chondrocyte to I) cluster formation.

signaling pathway [47–49]. Upon stimulation with 1 mM H_2O_2, p65 activation in chondrocytes was triggered due to IKK complex activation, which would induce phosphorylation and degradation of IκBα [50–52]. To further confirm whether CDP modulates NF-κB signaling activity *via* ROS scavenging, we treated CDP with H_2O_2 for 24 or 48 h. The results suggested that CDP significantly hindered the phosphorylation of IKK α and IKK β, while the transition trend of p65 was consistent with IKK. The phosphorylation of p65 in the H_2O_2 group was obstructed in the presence of CDP. The stability of CDP was still guaranteed, and the effect proved superior compared to only using clusterzymes. From the fluorescence comparison between H_2O_2 and group III (Fig. 5F), p65 nucleation was evidently inhibited, which further validates the earlier conclusion that CDP scavenges excessive ROS, returning the inflammatory joint microenvironment back to a normal state.

2.6. *In vivo* therapeutic efficacy of CDP

To examine the cartilage protective capability and sustained release characteristics of CDP in a living organism, we conducted tests using mature male New Zealand Rabbits. The animals were sorted into five groups, where we carried out bilateral anterior cruciate ligament transection (ACLT, n = 36) or a sham operation (n = 9) (Fig. S6, Supporting information) [53,54]. This model has been shown to alleviate osteoarthritis progression in a low ROS environment [55,56]. Four weeks post-surgery, we administered intra-articular injections of 100 μl 2.5 ng/μl CDP or its constituents (clusterzymes or PEG-DMSNs-NH_2) fortnightly, totaling two times. The positive groups were given 0.9 % sterile normal saline injections. For CDP can maintain high concentrations in the joint cavity within 2 weeks, while Clusterzyme is rapidly lost (Fig. S7, Supporting information), we picked two time points, 4 weeks and 8 weeks, to evaluate the sustained release impact of CDP. Additionally, we conducted a third round of experiments with the rabbits receiving delayed treatment, with the injections extending for another 4 weeks to examine the effectiveness of CDP and clusterzymes in more severe osteoarthritic conditions (Fig. 6A). The blood routine and biochemistry were monitored prior to each injection, and all joints were collected 2 weeks following the second injection. Before collecting the samples, we ran a 1.5T T2-weighting Magnetic Resonance Imaging (MRI) scan on the joint to investigate the form and thickness of the articular cartilage and the physiological structure of the arthrosis (Fig. 6B) [57].

The outcome of the *in vivo* experiment studying CDP's impact on cartilage preservation and sustained release was examined using MRI imagery. The investigation revealed that cartilage damage severity progressively escalated in the two groups of rabbits with OA—specifically the 4 weeks group and the 8 weeks group. The 4 weeks group displayed a minor discontinuity in the cartilage layer, which substantially worsened by the time of the 8 weeks group. In contrast, the delay-treated group exhibited completely worn-down articular cartilage, with an impaired joint structure. Adjusting the timing or concentration of administration also made a difference in efficacy. The PEG-DMSNs-NH_2 group didn't show any therapeutic effect, mirroring the results of the control group (Figs. S8 and S9, Supporting information).

On the other hand, the clusterzymes group showed a relatively intact joint structure, but there was discontinuity in the cartilage layer. However, compared to the groups for 4 and 8 weeks, the second half of the femoral head in the 8 weeks group was almost worn out, implying that after clusterzymes is depleted, it can no longer continue to protect the joints. Furthermore, joint wear continued to increase in the delay-treated group, which suggests that clusterzymes was unable to rescue or prevent further worsening of joint wear and tear.

Despite the minor discontinuity and wear of the articular cartilage observed in both the 8-week group and the delay-treated group, this could be considered irreversible early wear and tear prior to the application of CDP. With its slow-release feature, CDP displayed promising results in preventing the exacerbation of articular cartilage wear and tear, thus providing further protection for the cartilage. Hence, the sustained-release functionality ensured a prolonged duration of the therapeutic effect.

The protective properties of CDP on articular cartilage are more evident when observing the surface view of the femoral head (Fig. 6C). In comparison to the control and Group I, CDP shows minor cartilage wear and osteophyte development, providing compelling evidence of its therapeutic effectiveness. However, clusterzymes treatment only partially prevented cartilage wear, suggesting a somewhat limited protective benefit. When comparing the three groups based on time differences, it became clear that the delayed treatment also caused cartilage wear in Group III, though less extensive than in the control and Group I. Further structural variations of the femoral heads in each group were observed *via* H&E staining, substantiating the findings from the MRI images. The presence of osteophytes in the control and Group I aligns with the severity of arthritis observed in these groups, while the minimal cartilage wear in Group III underscores its therapeutic efficacy. Taken as a whole, the surface view of the femoral head and H&E staining (Fig. S10, supporting information) offer a well-rounded comprehension of CDP's protective effects on articular cartilage, and its potential as an osteoarthritis treatment. Thus, these findings suggest that CDP stands out as a potentially promising therapeutic agent for osteoarthritis management, granting protection to articular cartilage from wear and tear, and reducing osteophyte formation.

For deeper scrutiny of bone wear along with the observation of osteophytes and bone density, micro-CT was employed for measurements and comparative review (Fig. 6D). Osteophytes were noticed at different time points in both the control and Group I. An aspect not discernible by mere surface observation is the impact of matrix metalloproteinases (MMPs) on the equilibrium between osteoblasts and osteoclasts, resulting in excessive osteoclast activity and ensuing trabecular damage. It was evident when examining control and Group I that there was a substantial loss of trabecular bone, and Group II followed suit. However, the density of bone trabeculae in Group III echoed that of the sham group. The findings suggest that CDP effectively thwarted loss of bone density and osteophyte formation, indicating crucial improvement in bone health. The variance in bone density and microstructure across the different groups was corroborated further by histological analysis. The H&E staining results suggested significant differences in the trabecular bone's thickness and density among the groups. These findings provide supplementary evidence for CDP's protective effect on bone health in relation to osteoarthritis.

In our subsequent study, we probed the morphological and structural changes in the cartilaginous layer in the experimental groups (Fig. 6E). We utilized the OARSI histopathology initiative to ascertain the differences among the groups, conducting blinded histological scoring of Safranin O/fast green stained joint tissues (Fig. 6F–I) [58]. The results illuminated that early-stage CDP injections led to notable inhibition of proteoglycan loss, thereby helping maintain overall cartilage integrity [59]. We discovered that the cartilage layer in the control and Group I displayed severe structural damage and a loss of proteoglycan content, whereas Group II exhibited moderate improvement by comparison. Remarkably, the cartilage layer in Group III remained intact and displayed no notable signs of proteoglycan loss. These findings suggest, therefore, that CDP can effectively thwart the advancement of cartilage degradation and sustain the structural soundness of the joint.

In order to delve deeper into the underlying mechanics of CDP's chondroprotective function, we probed into the protective impact of CDP on cartilage by using a rabbit model of ACLT-induced osteoarthritis. Initially, we studied its biocompatibility *in vivo* (Figs. S11 and S12, Supporting Information). CDP treatment didn't exhibit any harmful effect on the primary organs of the animals as it was delivered *via* intra-articular injection. The results depicted that the ACLT model initiated an inflammatory phenotype, demonstrated by a decline in red blood cell count and a rise in white blood cell count. On top of this, heightened levels of alkaline phosphatase hinted at inflammation and bone damage.

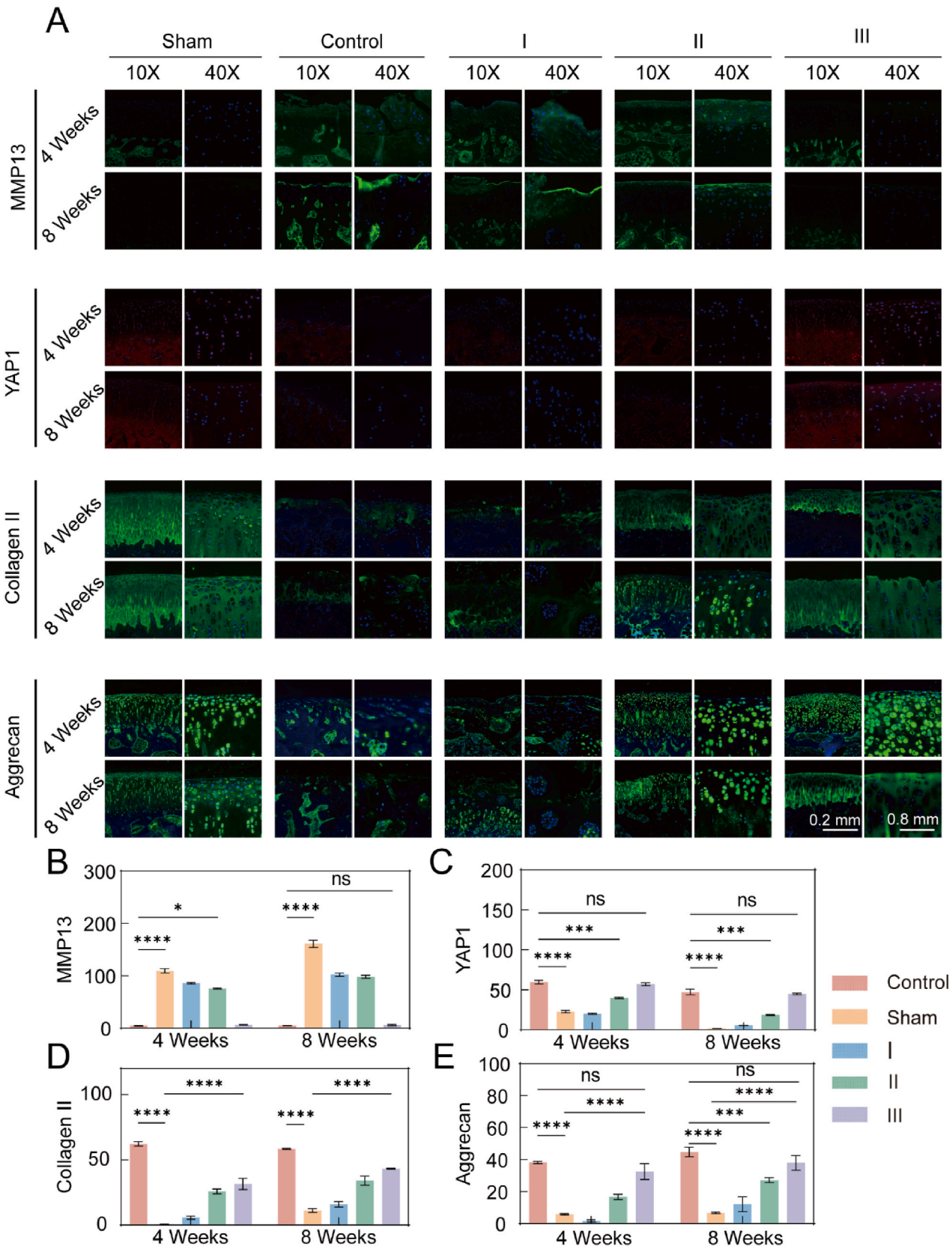

Fig. 7. A) immunofluorescence of MMP13, YAP1, collagen II and aggrecan. B) - E) quantitative analysis of IF, CDP acts as a protector of YAP1 and inhibitor of MMP13, resulting in block ROS to activate hippo pathway, which maintain the normal secretion of related proteins in cartilage. (*: $p < 0.05$, **: $p < 0.01$, ***: $p < 0.001$, ****: $p < 0.0001$).

Conversely, most of the blood evaluations and routine remained unaffected in OA, implying that the ACLT model specifically triggered an inflammatory response.

The abnormal values of blood routine and blood biochemistry were held within the normal range through YAP protection and inhibition of downstream NF-κB. However, the effects in the delay-treated groups, namely Group I or Group II, were more comparable to those of the control group, rather than Group III. This underlines the significance of the sustained-release function in maintaining chondroprotective function.

In the course of our animal experiments, we employed several commonly used clinical examination techniques, including micro-CT and MRI, to assess the extent of joint damage caused by arthritis. Micro-CT primarily focuses on evaluating the destruction of bone structure during the later stages of inflammation, while MRI is capable of detecting early cartilage degradation during the initial stages of inflammation [60]. The collection of these data is instrumental in facilitating the application of personalized treatments in clinical settings. By analyzing MRI evaluation results in conjunction with varying injection times or dosages, we can adjust drug dosages and better anticipate prognoses. Additionally, blood routine tests and biochemical inflammatory factor indicators can serve as valuable reference standards [61]. Nevertheless, more specific applications require further validation through accurate animal experiments or clinical studies; the methods discussed here are presented for consideration.

These variations were mirrored not just in the whole-body indicators, but also in the immunofluorescence of the arthrosis (Fig. 7A and Fig. S13, Supporting information). CDP works by inhibiting the degradation of YAP in the hippo pathway by eliminating ROS, leading to a decline in matrix metalloproteinases (MMPs), thereby protecting the cartilage. As per the statistical results of fluorescence intensity, it was observed that CDP demonstrated continuous and stable cartilage protection over a span of 8 weeks, a function that could not be matched by clusterzymes. Without the safeguarding of PEG-DMSNs-NH_2, clusterzymes would be rapidly cleared during articular movement.

Furthermore, compared to early treatment with CDP, the levels of YAP and MMP13 in groups treated later with CDP varied from the sham group (Fig. 7B and C). Considering that YAP degradation happens prior to CDP injection and given the role of CDP as ROS scavengers and YAP protectors, it ameliorates the inflammatory environment in the arthrosis cavity. Even so, CDP cannot reverse the degradation of YAP instigated by ROS and the inflammatory environment, thereby causing differences between the delay-treated groups and the sham groups. In the delay-treated groups [62], while YAP expression significantly diminished, it still remained higher than in the control groups. This suggests that CDP played an early role in safeguarding YAP, but in the later stages, the inflammatory environment still held sway, leading to the buildup of MMP13 [63]. By protecting YAP and clearing MMP13, the accumulation of collagen components in articular cartilage such as collagen II and aggrecan are preserved (Fig. 7D and E).

All in all, these discoveries indicate that CDP exhibits potent chondroprotective effects in the ACLT-induced osteoarthritis rat model. The mechanism of action involves safeguarding YAP and inhibiting NF-κB downstream. CDP also showcases stable and sustained cartilage protection over a period of 8 weeks, a trait not seen with clusterzymes. The spatiotemporal delivery function of CDP is critical for maintaining its chondroprotective function.

3. Conclusion

Our research developed a pH-dependent DMSNs system, loaded with Cu-doped clusterzymes, designed to protect articular chondrocytes by scavenging ROS and preventing YAP degradation in inflammatory environments. The system leverages the potential of YAP to inhibit downstream NF-κB pathways by preventing IKK activation. DMSNs come with well-developed biodegradation and biocompatibility, when loaded with clusterzymes, have an efficient ROS scavenging ability.

Utilizing the rich mesoporous structure of DMSNs, the CDP complex, although meager in quantity, boasts high efficiency and biosafety properties. Given these characteristics, CDP operates as a long-lasting ROS scavenger, reducing oxidative stress levels in chondrocytes under inflammation relief. It blocks the activation of the hippo pathway, and the subsequent YAP degradation.

Importantly, YAP challenges NF-κB signaling to control articular cartilage homeostasis. By intra-articular injection of CDP, we managed to scavenge ROS *in vivo*, preserving the cellular oxidative stress level and mitochondrial activity at healthy norms.

The inhibition of YAP degradation not only aids in protecting chondrocyte viability but also improves inflammation relief and curbs the accumulation of matrix metalloproteinase. These findings highlight the promise of pH-dependent DMSNs loaded with the ROS-scavenging clusterzyme system as potential inflammation inhibitors and chondrocyte protectors for OA treatment, as well as for other high ROS inflammatory diseases.

4. Materials and methods

A detailed description of experimental section is provided in Supporting **Information** Materials and Methods.

Ethics approval and consent to participate

The animal use protocol in this paper has been reviewed and approved by the Institutional Animal Care and Use Committee (IACUC), ZJCLA.

CRediT authorship contribution statement

Yang Jin: Writing – original draft, Visualization, Investigation, Formal analysis, Data curation. **Chuan Hu:** Writing – review & editing, Investigation, Formal analysis, Data curation. **Jiechao Xia:** Writing – review & editing, Formal analysis, Data curation. **Dingqi Xie:** Investigation, Data curation. **Lin Ye:** Methodology, Investigation, Formal analysis. **Xinyi Ye:** Investigation. **Li Jiang:** Writing – review & editing. **Honghai Song:** Methodology, Investigation. **Yutao Zhu:** Methodology, Investigation. **Sicheng Jiang:** Investigation. **Weiqing Li:** Investigation. **Weiming Qi:** Writing – review & editing. **Yannan Yang:** Writing – review & editing, Methodology, Investigation, Conceptualization. **Zhijun Hu:** Writing – review & editing, Conceptualization.

Declaration of competing interest

The authors declare that they have no known competing financial interests or personal relationships that could have appeared to influence the work reported in this paper.

Acknowldgement

This research was supported by the Natural Science Foundation of Zhejiang Province of China (No. LY22H060003). The National Natural Science Foundation of China (82470903 to LJ), the Natural Science Foundation of Zhejiang Province (LY24C110001 to LJ).

Appendix A. Supplementary data

Supplementary data to this article can be found online at https://doi.org/10.1016/j.bioactmat.2024.09.004.

References

[1] G. Wei, K. Lu, M. Umar, Z. Zhu, W.W. Lu, J.R. Speakman, Y. Chen, L. Tong, D. Chen, Risk of metabolic abnormalities in osteoarthritis: a new perspective to understand its pathological mechanisms, Bone Res 11 (1) (2023) 63.

[2] Y. Zhang, J.M. Jordan, Epidemiology of osteoarthritis, Clin. Geriatr. Med. 26 (3) (2010) 355–369.

[3] J.G. Quicke, P.G. Conaghan, N. Corp, G. Peat, Osteoarthritis year in review 2021: epidemiology & therapy, Osteoarthritis Cartilage 30 (2) (2022) 196–206.

[4] K. von der Mark, T. Kirsch, A. Nerlich, A. Kuss, G. Weseloh, K. Gluckert, H. Stoss, Type X collagen synthesis in human osteoarthritic cartilage. Indication of chondrocyte hypertrophy, Arthritis Rheum. 35 (7) (1992) 806–811.

[5] D. Pfander, B. Swoboda, T. Kirsch, Expression of early and late differentiation markers (proliferating cell nuclear antigen, syndecan-3, annexin VI, and alkaline phosphatase) by human osteoarthritic chondrocytes, Am. J. Pathol. 159 (5) (2001) 1777–1783.

[6] A. Mantovani, S. Sozzani, M. Locati, P. Allavena, A. Sica, Macrophage polarization: tumor-associated macrophages as a paradigm for polarized M2 mononuclear phagocytes, Trends Immunol. 23 (11) (2002) 549–555.

[7] M. Tamaddon, H. Gilja, L. Wang, J.M. Oliveira, X. Sun, R. Tan, C. Liu, Osteochondral scaffolds for early treatment of cartilage defects in osteoarthritic joints: from bench to clinic, Biomaterials translational 1 (1) (2020) 3–17.

[8] C. Sun, J. Kang, C. Yang, J. Zheng, Y. Su, E. Dong, Y. Liu, S. Yao, C. Shi, H. Pang, J. He, L. Wang, C. Liu, J. Peng, L. Liu, Y. Jiang, D. Li, Additive manufactured polyether-ether-ketone implants for orthopaedic applications: a narrative review, Biomaterials translational 3 (2) (2022) 116–133.

[9] H. Wei, E. Wang, Nanomaterials with enzyme-like characteristics (nanozymes): next-generation artificial enzymes, Chem. Soc. Rev. 42 (14) (2013) 6060–6093.

[10] P. Dydio, H.M. Key, A. Nazarenko, J.Y. Rha, V. Seyedkazemi, D.S. Clark, J. F. Hartwig, An artificial metalloenzyme with the kinetics of native enzymes, Science 354 (6308) (2016) 102–106.

[11] M. Liang, X. Yan, Nanozymes: from new concepts, mechanisms, and standards to applications, Acc. Chem. Res. 52 (8) (2019) 2190–2200.

[12] S. Sun, H. Liu, Q. Xin, K. Chen, H. Ma, S. Liu, X. Mu, W. Hao, S. Liu, Y. Gao, Y. Wang, J. Pei, R. Zhao, S. Zhang, X. Zhang, H. Wang, Y. Li, X.D. Zhang, Atomic engineering of clusterzyme for relieving acute neuroinflammation through lattice expansion, Nano Lett. 21 (6) (2021) 2562–2571.

[13] H. Liu, Y. Li, S. Sun, Q. Xin, S. Liu, X. Mu, X. Yuan, K. Chen, H. Wang, K. Varga, W. Mi, J. Yang, X.D. Zhang, Catalytically potent and selective clusterzymes for modulation of neuroinflammation through single-atom substitutions, Nat. Commun. 12 (1) (2021) 114.

[14] Y. Lin, J. Ren, X. Qu, Nano-gold as artificial enzymes: hidden talents, Adv. Mater. 26 (25) (2014) 4200–4217.

[15] H. Yang, Z. Yu, S. Ji, J. Yan, Y. kong, Q. Huo, Z. Zhang, Y. Niu, Y. Liu, Regulation of synovial macrophages polarization by mimicking efferocytosis for therapy of osteoarthritis, Adv. Funct. Mater. 32 (52) (2022).

[16] D. Shen, J. Yang, X. Li, L. Zhou, R. Zhang, W. Li, L. Chen, R. Wang, F. Zhang, D. Zhao, Biphase stratification approach to three-dimensional dendritic biodegradable mesoporous silica nanospheres, Nano Lett. 14 (2) (2014) 923–932.

[17] Y. Yang, S. Bernardi, H. Song, J. Zhang, M. Yu, J.C. Reid, E. Strounina, D.J. Searles, C. Yu, Anion assisted synthesis of large pore hollow dendritic mesoporous organosilica nanoparticles: understanding the composition gradient, Chem. Mater. 28 (3) (2016) 704–707.

[18] Y. Lu, Y. Yang, Z. Gu, J. Zhang, H. Song, G. Xiang, C. Yu, Glutathione-depletion mesoporous organosilica nanoparticles as a self-adjuvant and Co-delivery platform for enhanced cancer immunotherapy, Biomaterials 175 (2018) 82–92.

[19] C. Xu, C. Lei, Y. Wang, C. Yu, Dendritic mesoporous nanoparticles: structure, synthesis and properties, Angew Chem. Int. Ed. Engl. 61 (12) (2022) e202112752.

[20] L. Han, C. Tang, C. Yin, pH-responsive core–shell structured nanoparticles for triple-stage targeted delivery of doxorubicin to tumors, ACS Appl. Mater. Interfaces 8 (36) (2016) 23498–23508.

[21] D. Zhou, F. Zhou, S. Sheng, Y. Wei, X. Chen, J. Su, Intra-articular nanodrug delivery strategies for treating osteoarthritis, Drug Discov. Today 28 (3) (2023) 103482.

[22] R. Cheng, L. Jiang, H. Gao, Z. Liu, E. Makila, S. Wang, Q. Saiding, L. Xiang, X. Tang, M. Shi, J. Liu, L. Pang, J. Salonen, J. Hirvonen, H. Zhang, W. Cui, B. Shen, H. A. Santos, A pH-responsive cluster metal-organic framework nanoparticle for enhanced tumor accumulation and antitumor effect, Adv. Mater. 34 (42) (2022) e2203915.

[23] J. Li, L. Xie, W. Sang, W. Li, G. Wang, J. Yan, Z. Zhang, H. Tian, Q. Fan, Y. Dai, A metal-phenolic nanosensitizer performs hydrogen sulfide-reprogrammed oxygen metabolism for cancer radiotherapy intensification and immunogenicity, Angew Chem. Int. Ed. Engl. 61 (18) (2022) e202200830.

[24] X.-x. Fan, M.-z. Xu, E.L.-H. Leung, C. Jun, Z. Yuan, L. Liu, ROS-responsive berberine polymeric micelles effectively suppressed the inflammation of rheumatoid arthritis by targeting mitochondria, Nano-Micro Lett. 12 (1) (2020).

[25] A. Kienzle, S. Kurch, J. Schloder, C. Berges, R. Ose, J. Schupp, A. Tuettenberg, H. Weiss, J. Schultze, S. Winzen, M. Schinnerer, K. Koynov, M. Mezger, N.K. Haass, W. Tremel, H. Jonuleit, Dendritic mesoporous silica nanoparticles for pH-stimuli-responsive drug delivery of TNF-alpha, Adv. Healthcare Mater. 6 (13) (2017).

[26] P. Mora-Raimundo, D. Lozano, M. Benito, F. Mulero, M. Manzano, M. Vallet-Regi, Osteoporosis remission and new bone formation with mesoporous silica nanoparticles, Adv. Sci. (2021) e2101107.

[27] Y. Gao, N. Shao, Y. Pei, X.C. Zeng, Icosahedral crown gold nanocluster Au43Cu12 with high catalytic activity, Nano Lett. 10 (3) (2010) 1055–1062.

[28] T. Higaki, Y. Li, S. Zhao, Q. Li, S. Li, X.S. Du, S. Yang, J. Chai, R. Jin, Atomically tailored gold nanoclusters for catalytic application, Angew. Chem. 131 (25) (2019) 8377–8388.

[29] M. Huo, L. Wang, Y. Chen, J. Shi, Tumor-selective catalytic nanomedicine by nanocatalyst delivery, Nat. Commun. 8 (1) (2017) 357.

[30] B. Chu, Y. Qu, X. He, Y. Hao, C. Yang, Y. Yang, D. Hu, F. Wang, Z. Qian, ROS-Responsive camptothecin prodrug nanoparticles for on-demand drug release and combination of chemotherapy and photodynamic therapy, Adv. Funct. Mater. (2020) 2005918.

[31] A.D. Michael W. Heaven, Peter S. White, Kennedy M. Holt, Royce W. Murray, Crystal structure of the gold nanoparticle [N(C8H17)4][Au25(SCH2CH2Ph)18], J. Am. Chem. Soc. (2008) 130.

[32] G. Kresse, Efficient iterative schemes for ab initio total-energy calculations using a plane-wave basis set, Phys. Rev. B 54 (1996).

[33] a.Z.J.A. H. Pakiari, Nature and strength of M-S Bonds (M) Au, Ag, and Cu) in binary alloy gold clusters, J. Phys. Chem. A (2010) 9212–9221.

[34] J.A. Bolduc, J.A. Collins, R.F. Loeser, Reactive oxygen species, aging and articular cartilage homeostasis, Free Radic. Biol. Med. 132 (2019) 73–82.

[35] R. Yuan, Y. Li, S. Han, X. Chen, J. Chen, J. He, H. Gao, Y. Yang, S. Yang, Y. Yang, Fe-curcumin nanozyme-mediated reactive oxygen species scavenging and anti-inflammation for acute lung injury, ACS Cent. Sci. 8 (1) (2022) 10–21.

[36] Q. Yao, X. Wu, C. Tao, W. Gong, M. Chen, M. Qu, Y. Zhong, T. He, S. Chen, G. Xiao, Osteoarthritis: pathogenic signaling pathways and therapeutic targets, Signal Transduct. Targeted Ther. 8 (1) (2023) 56.

[37] Haruhiko Akiyama, P. Jon Lyons, Yuko Mori-Akiyama, Xiaohong Yang, Ren Zhang, Zhaoping Zhang, Jian Min Deng, Makoto M. Taketo, Takashi Nakamura, Richard R. Behringer, Pierre D. McCrea, Benoit de Crombrugghe, Interactions between Sox9 and ␣-catenin control chondrocyte differentiation, Gene Dev. (2004) 1072–1087.

[38] J. Guo, F. Wang, Y. Hu, Y. Luo, Y. Wei, K. Xu, H. Zhang, H. Liu, L. Bo, S. Lv, S. Sheng, X. Zhuang, T. Zhang, C. Xu, X. Chen, J. Su, Exosome-based bone-targeting drug delivery alleviates impaired osteoblastic bone formation and bone loss in inflammatory bowel diseases, Cell reports. Medicine 4 (1) (2023) 100881.

[39] P. Lepetsos, A.G. Papavassiliou, ROS/oxidative stress signaling in osteoarthritis, Biochim. Biophys. Acta (BBA) - Mol. Basis Dis. 1862 (4) (2016) 576–591.

[40] J. Jin, L. Zhang, X. Li, W. Xu, S. Yang, J. Song, W. Zhang, J. Zhan, J. Luo, H. Zhang, Oxidative stress-CBP axis modulates MOB1 acetylation and activates the Hippo signaling pathway, Nucleic Acids Res. 50 (7) (2022) 3817–3834.

[41] S. Zhang, B. Zhang, Z. Liao, Y. Chen, W. Guo, J. Wu, H. Liu, R. Weng, D. Su, G. Chen, Z. Zhang, C. Li, J. Long, Y. Xiao, Y. Ma, T. Zhou, C. Xu, P. Su, Hnrnpk protects against osteoarthritis through targeting WWC1 mRNA and inhibiting Hippo signaling pathway, Mol. Ther. (2024) 1461–1478.

[42] K. Sun, J. Guo, Z. Guo, L. Hou, H. Liu, Y. Hou, J. He, F. Guo, Y. Ye, The roles of the Hippo-YAP signalling pathway in Cartilage and Osteoarthritis, Ageing Res. Rev. 90 (2023) 102015.

[43] L. Fu, Y. Hu, M. Song, Z. Liu, W. Zhang, F.X. Yu, J. Wu, S. Wang, J.C. Izpisua Belmonte, P. Chan, J. Qu, F. Tang, G.H. Liu, Up-regulation of FOXD1 by YAP alleviates senescence and osteoarthritis, PLoS Biol. 17 (4) (2019) e3000201.

[44] Y. Deng, J. Lu, W. Li, A. Wu, X. Zhang, W. Tong, K.K. Ho, L. Qin, H. Song, K.K. Mak, Reciprocal inhibition of YAP/TAZ and NF-kappaB regulates osteoarthritic cartilage degradation, Nat. Commun. 9 (1) (2018) 4564.

[45] W. Hou, C. Ye, M. Chen, W. Gao, X. Xie, J. Wu, K. Zhang, W. Zhang, Y. Zheng, X. Cai, Excavating bioactivities of nanozyme to remodel microenvironment for protecting chondrocytes and delaying osteoarthritis, Bioact. Mater. 6 (8) (2021) 2439–2451.

[46] W.H. Robinson, C.M. Lepus, Q. Wang, H. Raghu, R. Mao, T.M. Lindstrom, J. Sokolove, Low-grade inflammation as a key mediator of the pathogenesis of osteoarthritis, Nat. Rev. Rheumatol. 12 (10) (2016) 580–592.

[47] P. Lepetsos, K.A. Papavassiliou, A.G. Papavassiliou, Redox and NF-κB signaling in osteoarthritis, Free Radic. Biol. Med. 132 (2019) 90–100.

[48] S. Rigoglou, A.G. Papavassiliou, The NF-κB signalling pathway in osteoarthritis, Int. J. Biochem. Cell Biol. 45 (11) (2013) 2580–2584.

[49] H. Chen, M. Tu, S. Liu, Y. Wen, L. Chen, Dendrobine alleviates cellular senescence and osteoarthritis via the ROS/NF-κB Axis, Int. J. Mol. Sci. 24 (3) (2023) 2365.

[50] A.e.a. Yaron, Identification of the receptor component of the IkappaBalpha-ubiquitin ligase, Nature 396 (1998) 590–594.

[51] Jeffrey T. Winston, Peter Strack, Peggy Beer-Romero, Claire Y. Chu, Stephen J. Elledge, J. Wade Harper, The SCFbeta-TRCP-ubiquitin ligase complex associates specifically with phosphorylated destruction motifs in IkappaBalpha and beta-catenin and stimulates IkappaBalpha ubiquitination in vitro, Genes Dev. 13 (1999) 270–283.

[52] J.J. Erika Spencer, Zhijian J. Chen, Signal-induced ubiquitination of IκBα by the F-box protein Slimb/␣-TrCP, Genes Dev. 13 (1999) 284–294.

[53] L. Huang, I. Riihioja, P. Tanska, S. Ojanen, S. Palosaari, H. Kröger, S.J. Saarakkala, W. Herzog, R.K. Korhonen, M.A.J. Finnilä, Early changes in osteochondral tissues in a rabbit model of post-traumatic osteoarthritis, J. Orthop. Res. 39 (12) (2021) 2556–2567.

[54] T.K.J.M. Wong, C.S. Jayadev, W. Khan, D. Johnstone, Anterior cruciate ligament rupture and osteoarthritis progression, Open Orthop. J. 6 (2012) 295–300.

[55] H. Zhang, L. Wang, J. Cui, X. Chen, J. Su, Maintaining hypoxia environment of subchondral bone alleviates osteoarthritis progression, Sci. Adv. (2023) eabo7868.

[56] Y. Wang, Y. Chen, Y. Wei, Osteoarthritis animal models for biomaterial-assisted osteochondral regeneration, Biomaterials translational 3 (4) (2022) 264–279.

[57] F.W. Roemer, S. Demehri, P. Omoumi, T.M. Link, R. Kijowski, S. Saarakkala, M. D. Crema, A. Guermazi, State of the Art: imaging of osteoarthritis—Revisited 2020, Radiology 296 (1) (2020) 5–21.

[58] S. Laverty, C.A. Girard, J.M. Williams, E.B. Hunziker, K.P.H. Pritzker, The OARSI histopathology initiative – recommendations for histological assessments of osteoarthritis in the rabbit, Osteoarthritis Cartilage 18 (2010) S53–S65.
[59] E.K.B.M.W. Lark, J. Flanagan, C.F. Harper, L.A. Hoerrner, N.I. Hutchinson, I. I. Singer, S.A. Donatelli, J.R. Weidner, H.R. Williams, R.A. Mumford, L. S. Lohmander, Aggrecan degradation in human cartilage. Evidence for both matrix metalloproteinase and aggrecanase activity in normal, osteoarthritic, and rheumatoid joints, J. Clin. Invest. 100 (1) (1997) 93–106.
[60] A.E. Fogarty, M.C. Chiang, S. Douglas, L.H. Yaeger, F. Ambrosio, C. Lattermann, C. Jacobs, J. Borg Stein, A.S. Tenforde, Posttraumatic osteoarthritis after athletic knee injury: a narrative review of diagnostic imaging strategies, Pm&R (2024). Epub ahead of print.
[61] T.A.T. Nurmirinta, M.J. Turunen, R.K. Korhonen, J. Tohka, M.K. Liukkonen, M. E. Mononen, Two-stage Classification of future knee osteoarthritis severity after 8 Years using MRI: data from the osteoarthritis initiative, Ann. Biomed. Eng. (2024). Epub ahead of print.
[62] S. Portal-Núñez, P. Esbrit, M.J. Alcaraz, R. Largo, Oxidative stress, autophagy, epigenetic changes and regulation by miRNAs as potential therapeutic targets in osteoarthritis, Biochem. Pharmacol. 108 (2016) 1–10.
[63] C.M. Mazur, J.J. Woo, C.S. Yee, A.J. Fields, C. Acevedo, K.N. Bailey, S. Kaya, T. W. Fowler, J.C. Lotz, A. Dang, A.C. Kuo, T.P. Vail, T. Alliston, Osteocyte dysfunction promotes osteoarthritis through MMP13-dependent suppression of subchondral bone homeostasis, Bone Res 7 (2019) 34.